Branched actin polymerization drives invasive protrusion formation to promote myoblast fusion during skeletal muscle regeneration

Yue Lu[1*], Tezin Walji[1], Pratima Pandey[1], Chuanli Zhou[2], Christa W. Habela[3], Scott B. Snapper[4], Rong Li[5,6], Elizabeth H. Chen[1,7,8,9*]

[1] Department of Molecular Biology, University of Texas Southwestern Medical Center, Dallas, TX, USA

[2] Department of Immunology, University of Texas Southwestern Medical Center, Dallas, TX, USA

[3] Department of Neurology, Johns Hopkins University School of Medicine, Baltimore, MD, USA.

[4] Department of Pediatrics, Boston Children's Hospital, Boston, MA, USA.

[5] Department of Cell Biology, Johns Hopkins University School of Medicine, Baltimore, MD, USA.

[6] Mechanobiology Institute, National University of Singapore, Singapore, Singapore.

[7] Department of Cell Biology, University of Texas Southwestern Medical Center, Dallas, TX, USA

[8] Hamon Center for Regenerative Science and Medicine, University of Texas Southwestern Medical Center, Dallas, TX, USA

[9] Harold C. Simmons Comprehensive Cancer Center, University of Texas Southwestern Medical Center, Dallas, TX, USA

* e-mail: Yue.Lu@UTSouthwestern.edu

* e-mail: Elizabeth.Chen@UTSouthwestern.edu

Abstract

Skeletal muscle regeneration is a multistep process involving the activation, proliferation, differentiation, and fusion of muscle stem cells, known as satellite cells. The fusion of satellite cell-derived mononucleated muscle cells (SCMs) is indispensable for the generation of multinucleated, contractile myofibers during muscle repair. However, the molecular and cellular mechanisms underlying SCM fusion during muscle regeneration remain poorly understood. In this study, we uncovered an essential role for branched actin polymerization in SCM fusion. Using conditional knockouts of the Arp2/3 complex and its actin nucleation-promoting factors, N-WASP and WAVE, we demonstrated that branched actin polymerization is required for the SCM fusion, but not for satellite cell proliferation, differentiation, and migration. We showed that the N-WASP and WAVE complexes have partially redundant functions in regulating SCM fusion. Furthermore, we showed that branched actin polymerization is essential for generating invasive protrusions at the fusogenic synapses in SCMs. Taken together, our study has identified new components of the myoblast fusion machinery in skeletal muscle regeneration and demonstrated a critical role for branched actin-propelled invasive protrusions in this process.

Introduction

Skeletal muscle is a unique tissue composed of elongated multinucleated cells known as myofibers (Grefte et al. 2007). In response to injury, skeletal muscle has the capacity to repair the injured myofiber in a process called muscle regeneration (Chen and Shan 2019). Muscle regeneration is dependent on the resident muscle stem cells, known as satellite cells (Relaix and Zammit 2012). Satellite cells are located between the myofiber plasma membrane and the basement membrane (BM), the latter of which is a layer of extracellular matrix material composed of collagen, glycoproteins, and proteoglycans (Seale et al. 2000; Webster et al. 2016). Satellite cells express high levels of Pax7, which is a paired domain-containing transcription factor, and remain quiescent under normal conditions (Le Grand and Rudnicki 2007; Cheung and Rando 2013; Yin et al. 2013). Upon injury, satellite cells are activated and then proliferate and differentiate into fusion-competent muscle cells. Once the satellite cell-derived muscle cells, which will be referred to as SCMs, fill the space within the BM remnants, known as ghost fibers, they would fuse with each other and/or with injured myofibers to regenerate the muscle (Le Grand and Rudnicki 2007; Lepper et al. 2009; Cheung and Rando 2013; Yin et al. 2013; Webster et al. 2016; Collins et al. 2024). SCM fusion occurs rapidly between day 3.5 to 5 post injury (dpi) and persists till ~dpi 10 (Collins et al. 2024). Despite the importance of SCM fusion in skeletal muscle regeneration, the molecular and cellular mechanisms underlying SCM fusion during muscle regeneration remain poorly understood. To date, only two proteins, the bi-partite myoblast fusogens myomaker (MymK) and myomixer (MymX)/myomerger/minion, have been shown to be required for SCM fusion (Millay et al. 2014; Bi et al. 2018). Identifying additional components of the SCM fusion machinery will not only facilitate our understanding of muscle regeneration but also provide more options to enhance muscle regeneration upon injury.

The Arp2/3 complex and its actin nucleation-promoting factors (NPFs), Neural Wiskott Aldrich Syndrome Protein (N-WASP) and WASP-family verprolin-homologous protein (WAVE), are known to generate branched actin filaments and have been shown to play a role in myoblast fusion during embryogenesis (Richardson et al. 2007; Gruenbaum-

Cohen et al. 2012). These actin regulators are required for generating invasive protrusions to promote plasma membrane juxtaposition and fusion at the fusogenic synapse (Sens et al. 2010; Luo et al. 2022; Lu et al. 2023). However, their potential function in muscle regeneration is completely unknown. Here, using satellite cell-specific knockout (KO) mice of Arp2/3 and NPFs, we show that branched actin polymerization is indispensable for muscle regeneration. In particular, Arp2/3 and NPFs are required for the formation of invasive protrusions during SCM fusion, but not satellite cell proliferation, differentiation or migration. Thus, we have identified new components of the SCM fusion machinery and demonstrated a critical function of branched actin-propelled invasive protrusions in skeletal muscle regeneration.

Results

The redistribution of muscle cells and macrophages at the early stage of skeletal muscle regeneration

To examine the behavior of muscle cells during fusion after injury, we injured the tibialis anterior (TA) muscles by $BaCl_2$ injection (Fig. 1A), and labeled the differentiating SCMs using anti-NCAM, a cell adhesion molecule highly expressed in these cells (Capkovic et al. 2008), and ghost fibers using anti-Laminin, a major component of the BM (Webster et al. 2016) (Fig. 1B). Since a previous study showed that macrophages are present in the ghost fiber to clear the necrotic debris of the damaged myofibers (Collins et al. 2024), we also labeled macrophages with anti-MAC-2, a member of lectin family expressed on macrophage cell-surface (Hohsfield et al. 2022).

At dpi 2.5, the differentiating SCMs and macrophages were two major cell populations residing within the ghost fibers, occupying 47.8% and 39.9% of the total volume, respectively. By dpi 3.5, SCMs occupied 98.2% of the ghost fiber volume, whereas macrophages only accounted for 1.8% (Fig. 1C), with most of the macrophages residing in the interstitial space outside of the ghost fibers (Fig. 1B). This would account for the high overall number of macrophages in the regenerating muscle tissues in this time period (Collins et al. 2024). How macrophages extravasated from the ghost fibers to the interstitial space remained an interesting question. Strikingly, our confocal (Fig. 2A and

Supplementary Video 1 & 2) and transmission electron microscopy (TEM) (Fig. 2B) analyses of regenerating TA muscles at dpi 3 revealed narrow openings (~1 μm diameter) on the BM of ghost fibers through which macrophages (MAC-2^{+}) with a ~20 μm diameter (as a round cell) were traversing, suggesting that the large macrophages squeeze through tiny openings on the BM to enter and/or escape the ghost fibers. The ability of macrophages to traverse the ghost fibers in and out makes it possible to spatiotemporally coordinate the ghost fiber occupancy by macrophages and SCMs during muscle regeneration.

Branched actin polymerization is required for mammalian skeletal muscle regeneration

Given that the Arp2/3 complex-mediated branched actin polymerization is required for myoblast fusion during mouse embryogenesis (Lu et al. 2023), we asked whether the Arp2/3 complex is required for skeletal muscle regeneration in adults. Toward this end, we generated satellite cell-specific, tamoxifen-inducible knockout mice for ArpC2, a subunit of the Arp2/3 complex (Goley and Welch 2006), by breeding *Pax7*^{CreERT2} with *ArpC2*$^{fl/fl}$ mice (Lepper et al. 2009; Wang et al. 2016). The conditional knockout (cKO) mouse line *Pax7*^{CreERT2}; *ArpC2*$^{fl/fl}$ will be referred to as *ArpC2*^{cKO} hereafter. The littermates of the *Pax7*^{CreERT2} male mice without the floxed *ArpC2* allele were used as wild-type controls. To induce genetic deletion of *ArpC2* in satellites, we performed intraperitoneal injection of tamoxifen to the control and mutant mice every two days over a period of ten days. satellite cell-specific *ArpC2* KO did not affect TA muscle weight and size in uninjured muscle (Fig. S1A-S1C). However, muscle injury by $BaCl_2$ resulted in a significant decrease (87.7 ± 2.0%) in the cross-section area (CSA) of regenerated myofibers in *ArpC2*^{cKO} mice compared to their littermate controls at dpi 14 (Fig. 3A-3C) and dpi 28 (Fig. S3A and S3B). Consistent with this, the frequency distribution of CSA displayed a significant shift toward the small size in the mutant mice (Fig. S2). Taken together, these data demonstrate that the Arp2/3-mediated branched actin polymerization is essential for skeletal muscle regeneration.

Branched actin polymerization is required for SCM fusion

To pinpoint the specific step of skeletal muscle regeneration – satellite cell proliferation, differentiation, migration, and SCM fusion – in which branched actin polymerization is required, we performed immunostaining using antibodies that mark different steps. These experiments revealed that the percentages of muscle cells positive for the proliferation marker (Ki67) and the muscle differentiation marker (MyoG) in the injured TA muscles were similar between control and *ArpC2*^{cKO} mice (Fig. S4A-S4E). In addition, live imaging analysis showed that the cultured *ArpC2* KO SCMs exhibited similar migration and cell-cell contact (Supplementary Video 3). Thus, branched actin polymerization is dispensable for the proliferation, differentiation, and migration of SCs during skeletal muscle regeneration. The reduced muscle size in the *ArpC2* mutant mice is therefore likely due to defects in SCM fusion.

Since SCM fusion is mostly completed at dpi 4.5 (Fig. 1B)(Collins et al. 2024), we examined the regenerating TA muscles of the control and *ArpC2*^{cKO} mice at this time point (Fig. 3D). While most of the SCMs within the ghost fibers had fused in the control animals, the ghost fibers in the *ArpC2*^{cKO} mice contained differentiated (NCAM^{+}) but mostly unfused SCMs that could be readily observed in cross sections, similar to those in the *Mymx*^{cKO} mice (Fig. 3E, 3F and Fig. S5B). Consistent with this, the frequency distribution of SCM number per ghost fiber displayed a dramatic shift toward higher numbers in the *ArpC2*^{cKO} mice (Fig. S5C). These results indicate that the actin cytoskeleton plays an essential role in SCM fusion as the fusogenic proteins. Interestingly, expression of the fusogenic proteins, MymK and MymX, was up-regulated in the TA muscle of these mice (Fig. S4F), suggesting that fusogen overexpression is not able to rescue the SCM fusion defect resulted from defective branched actin polymerization. Furthermore, cultured *ArpC2*^{KO} satellite cells exhibited a severe myoblast fusion defect despite normal differentiation (Fig. 3G-3I), and pharmacologically inhibiting Arp2/3 with CK666 had the same effects (Fig. S5D-3G). Taken together, these results demonstrate that branched actin polymerization is specifically required for SCM fusion during skeletal muscle regeneration.

N-WASP and WAVE families have partially redundant functions in regulating SCM fusion

Activation of the Arp2/3 complex requires the actin NPFs, including the WASP and WAVE family of proteins (Goley and Welch 2006). To examine their potential functions in mammalian muscle regeneration, we generated single and double cKO mice for N-WASP [the WASP family member with high expression in SCMs (Lu et al. 2023)] and CYFIP1 [a subunit of the WAVE complex (Chen et al. 2014)], respectively. *Pax7*^{CreERT2}*; N-WASP*$^{fl/fl}$ will be referred to as *N-WASP*^{cKO}, *Pax7*^{CreERT2}; *CYFIP1*$^{fl/fl}$ as *CYFIP1*^{cKO}, and *Pax7*^{CreERT2}; *N-WASP*$^{fl/fl}$; *CYFIP1*$^{fl/fl}$ as dcKO hereafter.

At dpi 14, immunostaining revealed a moderate but significant decrease of TA myofiber CSA by 48.2 ± 0.1% in *N-WASP*^{cKO} and 67.7 ± 3.3% in *CYFIP1*^{cKO} mice, respectively, compared to their littermate controls (Fig. 3B and 3C). The myofiber CSA of dcKO mice was further decreased by 80.9 ± 1.8%, comparable to the CSA deduction observed in the *ArpC2*^{cKO} mice (in which both N-WASP and WAVE could not exert their functions) (87.7 ± 2.0%) (Fig. 3B and 3C) and in the *Mymx*^{cKO} mice (89.3 ± 1.9%). Consistent with the reduction of myofiber size, the *N-WASP*^{cKO} and *CYFIP1*^{cKO} single KO mice exhibited moderate myoblast fusion defects at dpi4, which were exacerbated in dcKO mice (Fig. 3E and 3F), despite normal satellite cell proliferation and differentiation, as well as fusogenic protein upregulation in the dcKO mice (Fig. S4A-S4F). Thus, our data have revealed partially redundant functions between N-WASP and WAVE NPFs in promoting myoblast fusion during skeletal muscle regeneration.

Branched actin polymerization promotes invasive protrusion formation during SCM fusion

To investigate the mechanism by which branched actin polymerization regulates SCM fusion during muscle regeneration, we first examined the cellular structure at the fusogenic synapse of cultured SCMs. Live cell imaging of cultured SCMs expressing LifeAct-mScarleti (mScar) and Arp2-mNeongreen (mNG) at day two in differentiation medium (DM) revealed Arp2- and F-actin-enriched finger-like protrusions projecting from the invading cells into their fusion partners (receiving cells), prior to cell membrane

fusion (Fig. 4A and Supplementary Video 4). Consistent with this, TEM analysis of TA muscle at dpi 3.5 in wild-type mice revealed invasive finger-like protrusions at muscle cell contact sites (28.7 ± 3.9% of SCMs exhibited invasive protrusions, n = 83 SCMs from 20 ghost fibers examined) (Fig. 4B and 4C). The average length and width of the finger-like protrusions were 422 ± 200 nm (n = 32 invasive protrusions) and 121 ± 73 nm (n = 32 invasive protrusions), respectively (Fig. S6A and S6B). In contrast, the muscle cells in *ArpC2*^{cKO} mice seldom formed invasive protrusions (1.4 ± 0.7% of the muscle cells exhibited invasive protrusions, n = 147 SCMs from 20 ghost fibers examined) (Fig. 4B), whereas protrusions in SCMs of *MymX*^{cKO} mice appeared normal (n = 29 invasive protrusions) (Fig. 4B, 4C, Fig. S6A and S6B). Therefore, branched actin polymerization, but not the fusogenic protein MymX, is required for invasive protrusion formation to promote myoblast fusion during adult muscle regeneration.

Discussion

In this study, we show that the Arp2/3 complex-mediated branched actin polymerization is indispensable for SCM fusion, but not for satellite cell proliferation, migration, or differentiation during muscle regeneration. The Arp2/3 NPFs, N-WASP and WAVE, exhibit partially redundant functions in regulating SCM fusion. Our live cell imaging and electron microcopy analysis revealed actin-propelled invasive protrusions at the fusogenic synapses of SCMs and a requirement for branched actin polymerization in generating these protrusions. Taken together, we propose that branched actin polymerization promotes mammalian muscle regeneration by generating invasive protrusions at the fusogenic synapse (Fig. 4D).

Studies in multiple organisms, including *Drosophila*, zebrafish, and mouse, have demonstrated that myoblast fusion during embryogenesis is mediated by actin-propelled invasive membrane protrusions (Sens et al. 2010; Chen 2011; Kim et al. 2015a; Kim and Chen 2019; Lee and Chen 2019; Luo et al. 2022; Lu et al. 2023). These protrusions serve several functions, including enhancing the plasma membrane contact areas between the fusion partners, increasing the mechanical tension of the fusogenic

synapse, and bringing the two opposing cell membranes into close proximity to engage the fusogenic proteins (Sens et al. 2010; Shilagardi et al. 2013; Kim et al. 2015b). The current study is the first revealing invasive protrusions as an integral part of the fusion machinery in adult skeletal muscle regeneration. In addition, we have identified molecular determinants of the invasive protrusions – the Arp2/3 complex and its NPFs, N-WASP and WAVE. It is striking that depleting the branched actin polymerization machinery results in a similarly severe SCM fusion defect as does depleting the fusogenic protein MymX, highlighting the crucial role for actin cytoskeletal rearrangements in SCM fusion. Indeed, our previous work using a reconstituted cell-fusion culture system in *Drosophila* revealed that fusogens and branched actin regulators are two minimal components of the cell-cell fusion machinery, and that actin-propelled invasive protrusions are required for fusogen engagement across the two apposing cell membranes (Shilagardi et al. 2013). It will be interesting to determine whether invasive protrusions promote the trans-interactions of fusogens at the mammalian fusogenic synapse.

We show in this study, for the first time, that macrophages can squeeze through tiny openings on the basement membrane to infiltrate and/or evacuate the ghost fibers during muscle regeneration. It is unclear whether these openings are small tears due to muscle injury or generated by macrophages through their interactions with the basement membrane. Carman et al. reported that lymphocytes use invasive podosomal protrusions to palpate the surface of, and ultimately generate transcellular pores through, the endothelium in a process called diapedesis (Carman et al. 2007). Given that macrophages can also generate invasive protrusions (Faust et al. 2019), it is conceivable that macrophages may use these invasive structures to push apart the protein meshwork on the basement membrane and thus opening small holes to get in and out of the ghost fibers. This feature would allow macrophages to infiltrate relatively intact basement membranes during micro muscle injuries to clear the debris and allow satellite cell proliferation and SCM fusion. Future studies are required to identify the mechanisms by which macrophages traverse the basement membrane during muscle regeneration.

Materials and Methods

Mouse Genetics

All animals were maintained under the ethical guidelines of the UT Southwestern Medical Center Animal Care and Use Committee according to NIH guidelines. C57BL/6J (stock: 000664) and *Pax7*^{CreERT2} (stock: 017763) mice were obtained from The Jackson Laboratory. The *ArpC2*$^{fl/fl}$ (Wang et al. 2016), *N-WASP*$^{fl/fl}$ (Cotta-de-Almeida et al. 2007), and *CYFIP1*$^{fl/fl}$ (Habela et al. 2020) mice were previously described. The *MymX*$^{fl/fl}$ line (Bi et al. 2018) was generously provided by Dr. Eric Olson. The control and mutant male littermates were used in each cohort of experiments.

Tamoxifen and $BaCl_2$-Induced Muscle Injury

Tamoxifen (Sigma; T5648) was dissolved at 20 mg/ml in corn oil. 100 µl tamoxifen/corn oil solution was administered by intraperitoneal injection to 2-month-old male mice as schematized in Figs. 3A, 3D, S1A, S3A, S4A and S5A. To induce muscle injury, $BaCl_2$ (Sigma; 342920) was dissolved in sterile saline to a final concentration of 1.2%, aliquoted, and stored at −20°C. Mice were anesthetized by isoflurane inhalation, the legs were shaved and cleaned with alcohol, and TA muscles were injected with 50 µL of $BaCl_2$ with a 28 gauge needle.

Satellite Cell Isolation and Culture

Satellite cells were isolated from limb skeletal muscles of 2-month-old male mice. Briefly, muscles were minced and digested in 800U/ml of type II collagenase (Worthington; LS004196) in F-10 Ham's medium (ThermoFisher Scientific; 11550043) containing 10% horse serum for 90 minutes at 37□°C with rocking to dissociate muscle fibers and dissolve connective tissues. The dissociated myofiber fragments were collected by centrifugation and digested in 0.5U/ml dispase (Gibco; 17105041) in F-10 Ham's medium for 30 minutes at 37□°C with rocking. Digestion was stopped with F-10 Ham's medium containing 20% FBS. Cells were then filtered from debris, centrifuged and resuspended in growth medium (GM: F-10 Ham's medium supplemented with 20% FBS, 4□ng/□ml FGF2, 1% penicillin–streptomycin and 10mM HEPEs). The cell suspension

from each animal was pre-plated twice on the regular 100 mm tissue culture-treated dishes for 30 minutes at 37 °C to eliminate fibroblasts. The supernatant containing mostly myoblasts was then transferred into collagen-coated dishes for culture in GM. To induce myogenic differentiation, satellite cells were cultured in DM (DMEM supplemented with 2% horse serum, 1% penicillin-streptomycin and 10mM HEPEs).

Pharmacological Treatments of Satellite Cells

To pharmacologically inhibit branched actin polymerization in SCMs, the Arp2/3 inhibitor CK666 (50 μM) were added into the DM at day 0 of differentiation of wild-type SCMs. After 48 hours, the cells were fixed in 4% paraformaldehyde (PFA) and stained with anti-MHC and DAPI to assess their differentiation and fusion index.

To delete *ArpC2* in satellite cells *in vitro*, satellite cells isolated from *ArpC2*^{cKO} mice were cultured in GM supplemented with or without 2 μM 4-hydroxytamoxifen (Sigma; H6278) for 10 days. Subsequently, the cells were trypsinized and plated at 70% confluency in DM. After 48 hours, the cells were fixed in 4% PFA and stained with anti-MHC and DAPI to assess their differentiation and fusion index.

Retroviral Vector Preparations and Expression

The LifeAct-mScarleti and Arp2-mNeongreen constructs were described in the previous study (Lu et al. 2023), and assembled into the retroviral vector pMXs-Puro (Cell Biolabs; RTV-012) using the NEBuilder HiFi DNA Assembly Cloning Kit (NEB; E2621L). To package the retrovirus, two micrograms of retroviral plasmid DNA was transfected into platinum-E cells (Cell Biolabs; RV-101) using the FuGENE HD transfection reagent. Two days after transfection, the virus-containing medium was filtered and concentrated with Retro-X Concentrator (Clontech, PT5063-2) following the manufacturer's protocol. The concentrated retroviruses were diluted in GM (with a 1:1000 dilution), mixed with polybrene (7 μg/ml), and used to infect cells. One day after infection, cells were washed with PBS and cultured in fresh GM.

Immunohistochemistry

To co-stain NCAM, MAC-2, and Laminin, the 4% PFA fixed TA muscles were dehydrated in 30% sucrose at 4°C overnight. The specimens were embedded in Tissue-Plus O.C.T. Compound (Fisher Scientific; 23-730-571) and 12-µm cryosections were collected onto Superfrost Plus Microscope Slides (Fisher Scientific;12-550-15). Then, the cryosections were incubated with blocking buffer for 20 minutes at room temperature (RT), followed by overnight incubation with rabbit anti-NCAM (1:200; Millipore; AB5032), rat anti-MAC-2 (1:200; Biolegend; 125401), and rat anti-Laminin-2 (1:500; Sigma; L0663) at 4°C. To stain for dystrophin, the freshly dissected TA muscles were snap frozen in Tissue-Plus O.C.T. Compound and 12-µm cryosections were collected onto Superfrost Plus Microscope Slides. Next, the sections were fixed in 4% PFA for 12 minutes at RT, washed three time with PBS and incubated with blocking buffer for 20 minutes at RT, followed by overnight incubation with rabbit anti-dystrophin (1:200; Abcam; ab15277) at 4°C. To co-stain Pax7, MyoG, Laminin, and Ki67, the freshly dissected TA muscles were snap frozen in Tissue-Plus O.C.T. Compound and 12-µm cryosections were collected onto Superfrost Plus Microscope Slides. Then, the sections were fixed in 2% PFA for 5 minutes at RT, washed three time with PBS and incubated with blocking buffer supplemented with M.O.M blocking reagent (1:25; Vector; MKB-2213-1) for 60 minutes at RT, followed by overnight incubation with mouse anti-Pax7 (1:2; DSHB; Pax7), mouse anti-MyoG (1:2; DSHB; F5D), rat anti-Laminin-2 (1:500; Sigma; L0663), and rat anti-Ki67 (1:500; ThermoFisher Scientific; 14-5698-82) at 4°C. After the incubation with primary antibodies, the sections were extensively washed with PBS and then incubated with alexa fluor-conjugated secondary antibodies for one hour at RT. Subsequently, the sections were washed with PBS and subjected to imaging using a Leica TCS SP8 inverted microscope. Reconstruction of z-stacks to 3-dementional images was performed using Imaris 10.1.

Western Blot

For western blots, proteins were isolated from TA muscle using ice-cold RIPA buffer (150mM NaCl, 1% NP40, 0.1% SDS and 50mM Tris, PH7.4) containing protease and phosphatase inhibitors (Cell Signaling Technologies; 5872) for 20 minutes. The supernatants were collected by centrifugation at 140,000 x g for 15 minutes. Protein

concentrations were determined using the Bradford Protein Assay Kit (Bio-Rad; 5000201). 10-30 µg total protein was loaded for each sample and separated by 10% SDS-PAGE gel and transferred to PVDF membranes (Millipore; GVHP29325). Then, the membranes were blocked for one hour at RT in PBS containing 5% nonfat dry milk and 0.1% Tween-20 (PBSBT) and subsequently were incubated with primary antibodies diluted at 1:1000 in PBSBT overnight at 4°C. The membranes were then washed with PBST and incubated with appropriate HRP-conjugated secondary antibodies diluted in PBSBT for one hour at RT. After extensive washes with PBST, the membranes were developed with the ECL western blotting substrate (ThermoFisher Scientific; 32209). The following primary antibodies were used: sheep anti-ESGP/MymX (1:1000; R&D Systems; AF4580), mouse anti-MymK (Zhang et al. 2020) (1:1000), and rabbit anti-β-Tubulin (1:1000; Cell Signaling Technologies; 2146).

Time-lapse Imaging and Analysis

Time-lapse imaging of cells incubated in 5% CO_2 at 37□°C was performed on a Nikon A1R confocal microscope with a Nikon Biostation CT. The satellite cells were seeded on fibronectin-coated cover glass (MATTEK; P35G-0-14-C) and imaged using a 40× (0.4 NA) objective at indicated time points after switching from GM to DM. The cells were imaged at two- or five-minute interval. After time-lapse imaging, ImageJ (NIH, 64-bit Java 1.8.0_172) was used to project the z-stacks in 2D, using maximum intensity projection and the resulting 2D images were assembled into a time-lapse video.

Electron Microscopy

To observe the invasive protrusions at the contact sites of SCMs during muscle regeneration *in vivo*, TA muscle at dpi 3.5 were fixed in a solution containing 3% paraformaldehyde, 2% glutaraldehyde, 1% sucrose, 3mM $CaCl_2$ in 0.1M sodium cacodylate buffer (pH 7.4) overnight at 4°C. Samples were subsequently washed with 0.1M cacodylate buffer containing 3% sucrose and 3mM $CaCl_2$, and post fixed with 1% osmium tetroxide in 0.1M sodium cacodylate buffer for 1.5 hours on ice. The muscle samples were stained with 2% uranyl acetate, dehydrated and embedded in EPON resin as previously described (Zhang and Chen 2008). The embedded samples were

then cut into 70-nm thick sections using LEICA ultramicrotome (UC6) and collected on copper slot grids. These sections were post-stained with 2% uranyl acetate and sato's lead solution and examined using a JEOL 1400 transmission electron microscope.

Statistics and Reproducibility

Statistical significance was assessed using two-tailed student's t-test. The *P* values were obtained using GraphPad Prism 8. The numbers of biological replicates for each experiment are indicated in the figure legends.

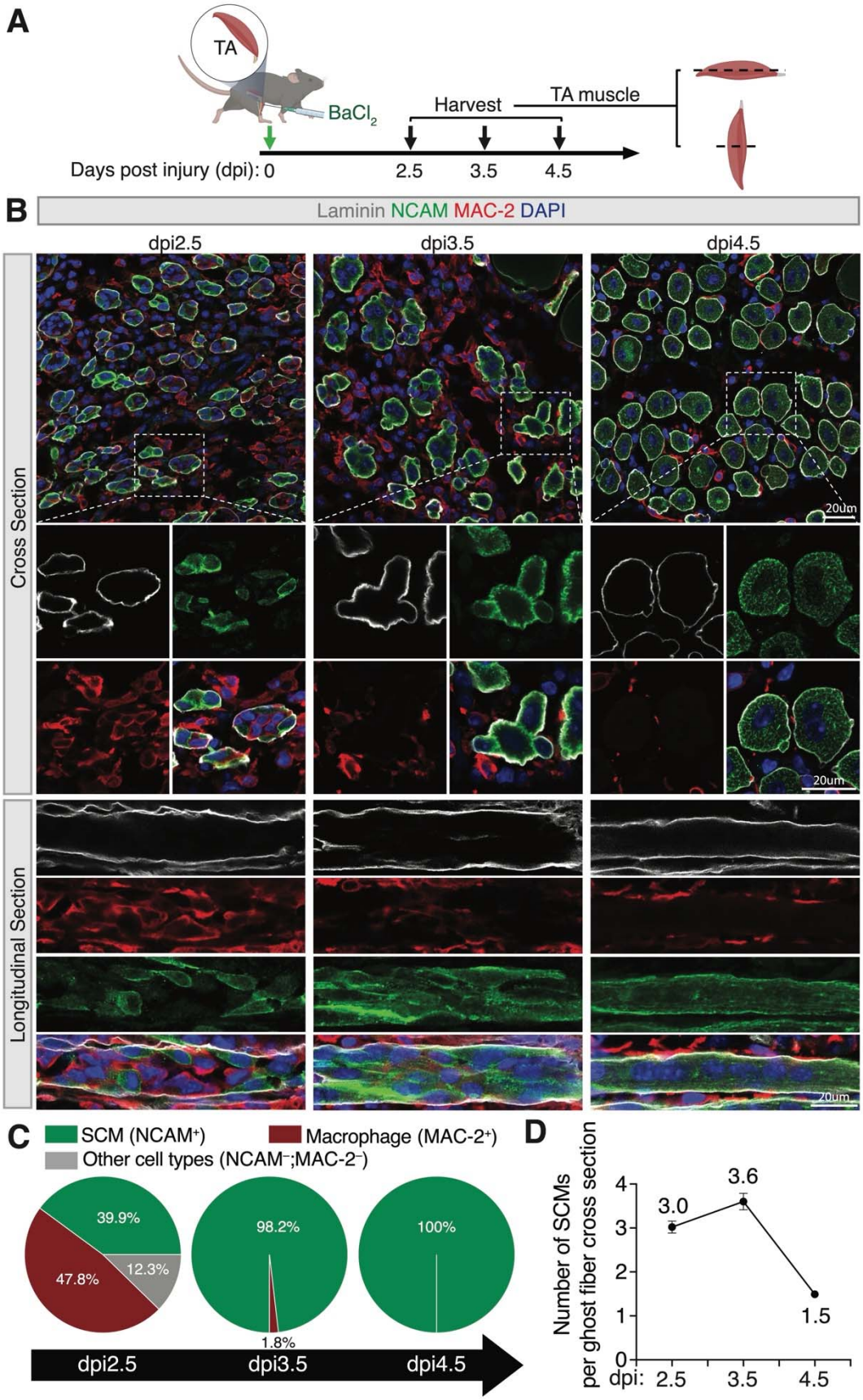

Figure 1. Spatiotemporal coordination of macrophages and SCMs during skeletal muscle regeneration

(A) Diagram of the TA muscle injury scheme. The TA muscles of the wild-type mice were injured by intramuscular injection of $BaCl_2$. The injured TA muscles were collected at dpi 2.5, 3.5, and 4.5 for cross and longitudinal sectioning and immunostaining.

(B) Immunostaining with anti-Laminin, anti-NACM, and anti-MAC-2 of the cross sections of TA muscles at the indicated time points. Note the decrease in the macrophage number within the ghost fiber at dpi 3.5 (compare to dpi 2.5), and the fusion of SCMs between dpi 3.5 and 4.5. Scale bars: 20 μm.

(C) Quantification of the percentage of macrophages and differentiated SCMs within ghost fibers at the indicated time points.

(D) Quantification of the number of differentiated SCMs in the cross sections of ghost fibers at the indicated time points.

For (C) and (D), *n* = 3 mice were analyzed for each time point and >500 ghost fibers in each mouse were examined. Mean and mean ± s.d. are shown in (C) and (D) , respectively.

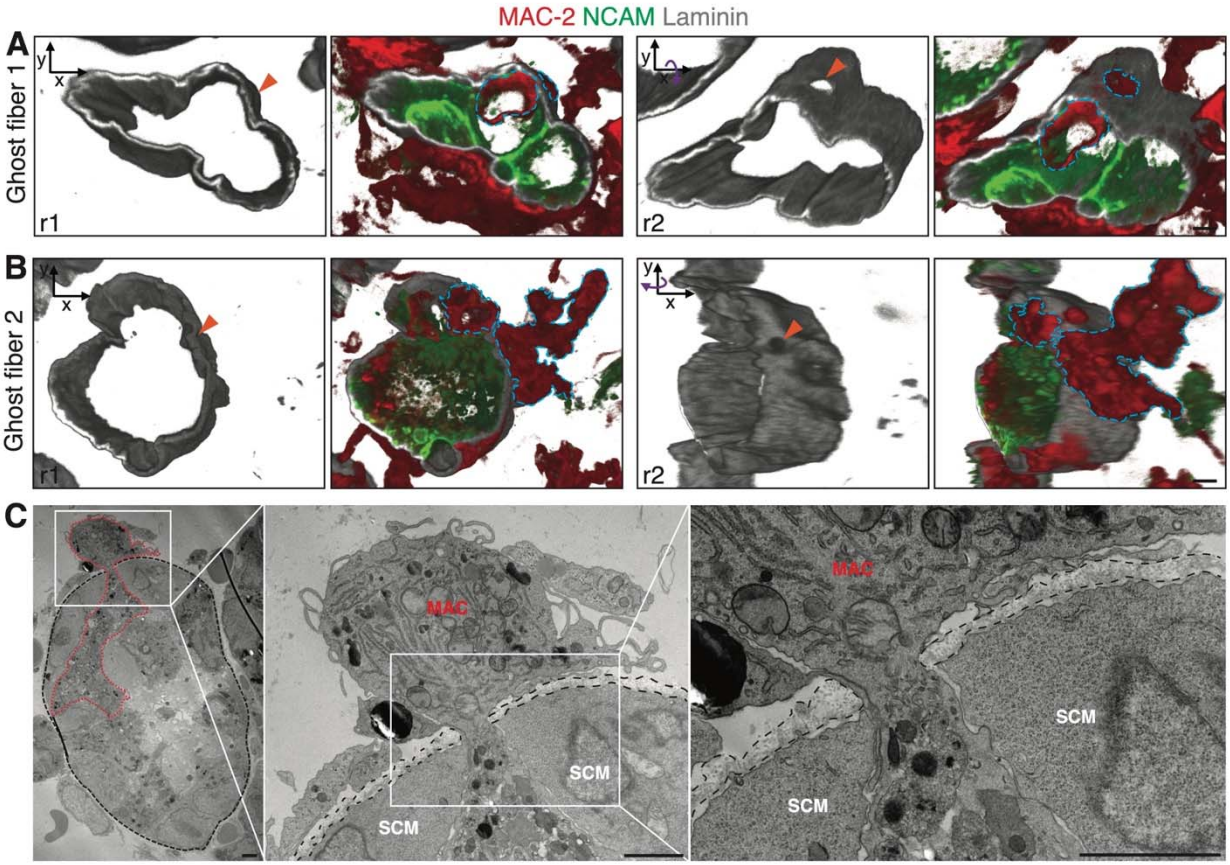

Figure 2. Macrophages extravasate the ghost fibers by traversing the BM

(A and **B)** Macrophages traversing the BM of ghost fibers shown by confocal microscopy. TA muscle cross sections of wild-type mice at dpi 3 were immunostained with anti-laminin, anti-NCAM, and anti-MAC-2, followed by confocal imaging. The confocal z-stacks were reconstructed to 3D images. Two examples are shown here. For each traversing macrophage (delineated by cyan dotted lines), images at two rotational angles are shown (r1 and r2). Note the small opening (arrowhead) on the BM through which a macrophage was passing (see supplementary video 1 & 2**)**.

(C) Macrophages traversing the BM of ghost fibers shown by TEM. The TA muscles as described in (**A**) and (**B**) were subjected to TEM processing. The BM is outlined by black dotted lines. The traversing macrophage is delineated by red dotted lines in the left panel. MAC: macrophage; SCM: SC-derived muscle cell. Scale bars: 2 μm.

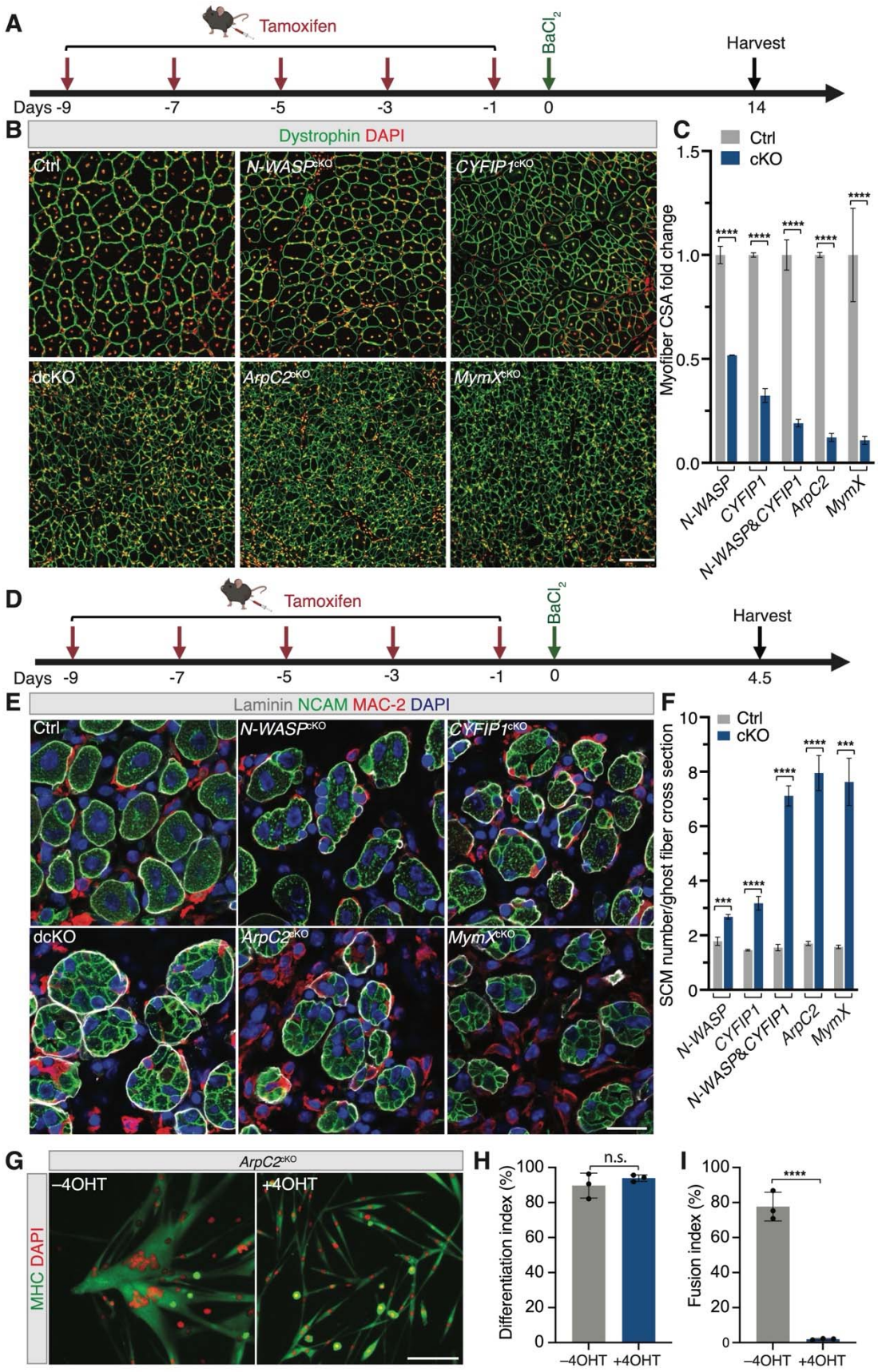

Figure 3. Branched actin polymerization is required for SCM fusion and skeletal muscle regeneration

(A) Schematic diagram of tamoxifen and $BaCl_2$ treatment and subsequent CSA analysis at dpi 14.

(B) Dystrophin and DAPI staining of the cross sections of TA muscles at dpi 14 from the control (Ctrl) and mutant mice. Note that the myofiber CSA is moderately decreased in *N-WASP*^{cKO} and *CYFIP1*^{cKO} mice, and severely reduced in dcKO, *ArpC2*^{cKO} and *MymX*^{cKO} mice. Scale bar: 100 μm.

(C) Quantification of the myofiber CSA in mutant vs. control mice.

(D) Schematic diagram of tamoxifen and $BaCl_2$ treatment and subsequent SCM number analysis at dpi 4.5.

(E) Immunostaining with anti-laminin, anti-NCAM, and anti-MAC-2 of the cross sections of TA muscles at dpi 4.5 from the control and mutant mice. Note that each ghost fiber in the control mice contained 1-2 centrally nucleated myofiber at dpi 4.5, indicating the near completion of SCM fusion. The ghost fibers in *N-WASP*^{cKO} and *CYFIP1*^{cKO} mice contained more SCMs, indicating impaired SCM fusion. Note that even more SCMs were seen in dcKO, *ArpC2*^{cKO} and *MymX*^{cKO} mice. Scale bar: 20 μm.

(F) Quantification of the SCM number per ghost fiber cross section in the control and mutant mice at dpi 4.5.

(G) ArpC2 is required for SCM fusion in cultured cells. The SCs isolated from ArpC2^{cKO} mice were maintained in GM without or with 2 μM 4OH-tamoxifen (4OHT) for 10 days. Subsequently, the cells were plated at 70% confluence in GM. After 24 hours, the cells were cultured in DM for 48 hours, followed by immunostaining with anti-MHC and DAPI. Note the robust fusion of the control (–4OHT) SCMs and the severe fusion defects in *ArpC2* KO (+4OHT) SCMs. Scale bar: 100 μm.

(H-I) Quantification of the differentiation index (% of nuclei in MHC$^+$ cells *vs*. total nuclei) and fusion index (% of nuclei in MHC$^+$ myotubes with ≥ 3 nuclei *vs*. total nuclei) of the two types of cells shown in (G). $n = 3$ independent experiments were performed.

For (**C** and **F**), $n = 3$ mice were analyzed for each time point and >500 ghost fibers in each mouse were examined. Mean ± s.d. values are shown in the bar graphs, and

significance was determined by two-tailed student's t-test. ***: $p < 0.001$; ****: $p < 0.0001$; n.s: not significant.

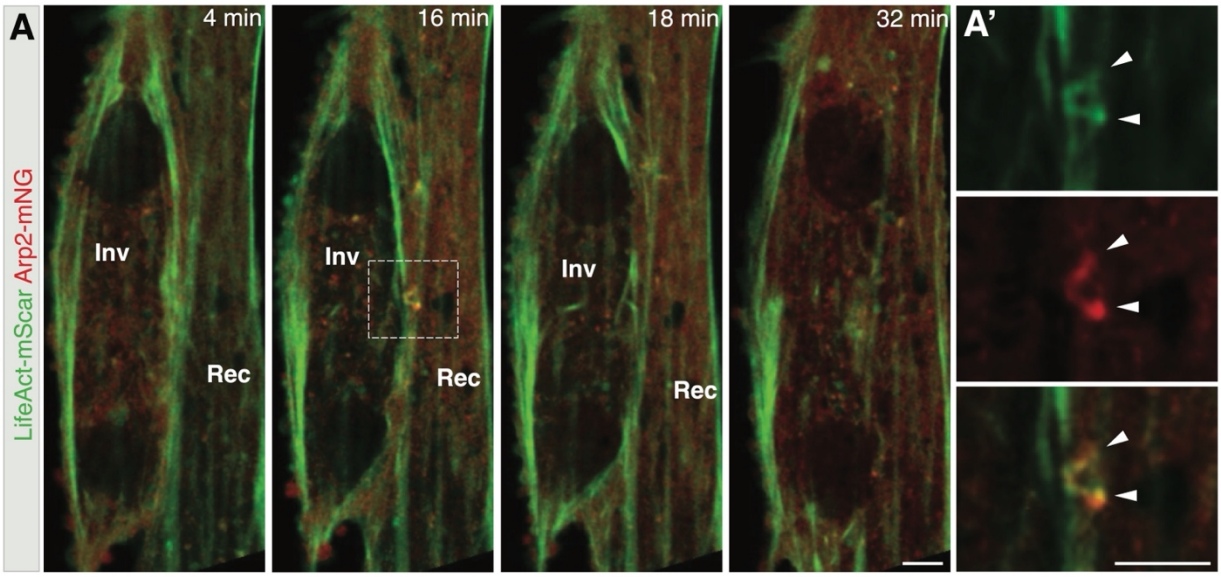

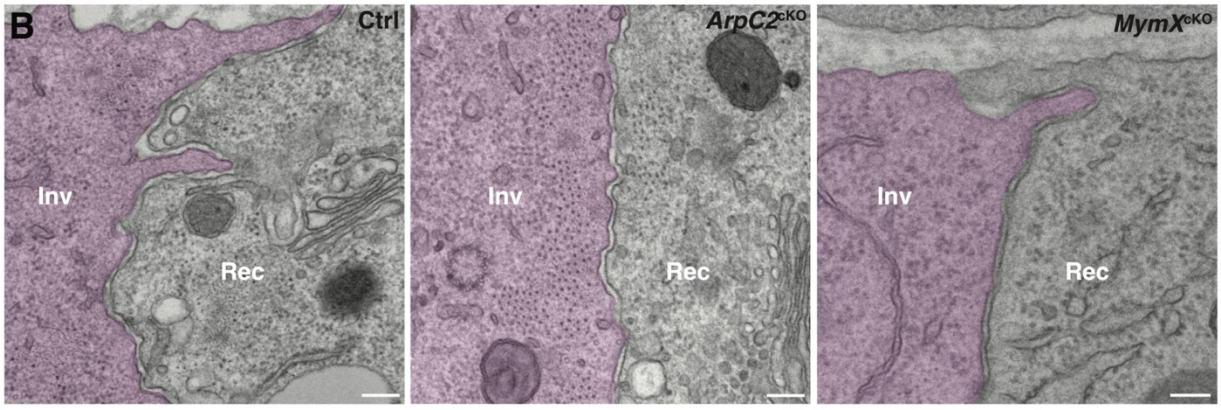

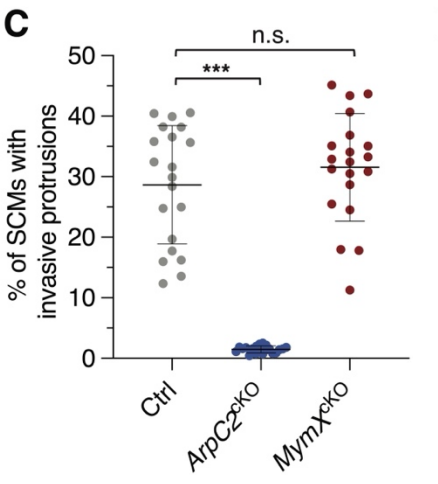

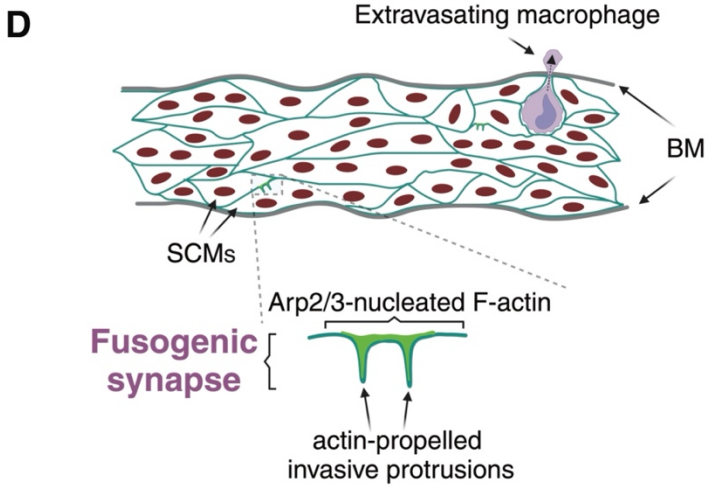

Figure 4. Branched actin polymerization is required for invasive protrusion formation during SCM fusion

(A) Still images of a fusion event between two LifeAct-mScar and Arp2-mNG co-expressing SCMs (see Supplemental Video 4). The boxed area is enlarged in (**A'**). Note the presence of two invasive protrusions (16 minute, arrowheads) enriched with LifeAct-mScar and Arp2-mNG at the fusogenic synapse. *n* = 8 fusion events were observed with similar results. Scale bar: 5 μm.

(B) TEM of TA muscle cells in wild-type control, *ArpC2*^{cKO}, and *MymX*^{cKO} mice at dpi 3.5. The invading SCMs are pseudo-colored in light magenta. Note the invasive membrane protrusions projected by SCMs in control and *MymX*^{cKO}, but not in the *ArpC2*^{cKO}, mice. Scale bars: 500 nm.

(C) Quantification of the percentage of SCMs generating invasive protrusions in the mice with genotypes shown in (**B**) at dpi 3.5. At least 83 SCMs from n = 20 ghost fibers in each genotype were quantified. Mean ± s.d. values are shown in the dot plots, and significance was determined by two-tailed student's t-test. ***p < 0.001; n.s: not significant.

(D) A model depicting the function of Arp2/3-mediated branched actin polymerization in promoting invasive protrusion formation and SCM fusion during skeletal muscle regeneration.

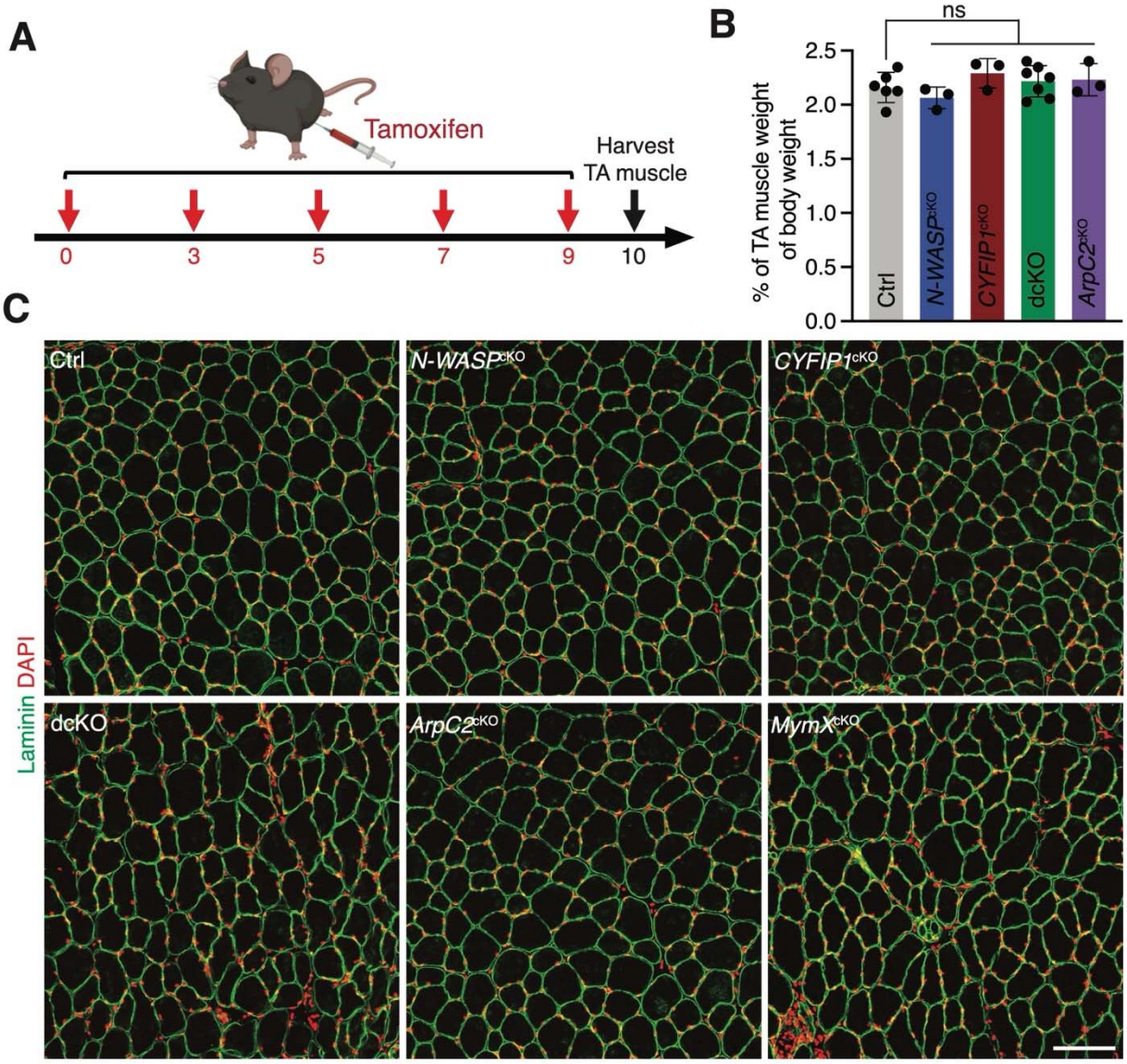

Supplementary Figure 1. The TA muscle weight and size are not affected by SC-specific deletion of branched actin polymerization regulators before injury

(A) Schematic diagram of tamoxifen treatment and TA muscle harvest.

(B) Quantification of the TA muscle weight. Mice with the indicated genotypes were treated as described in (A). The whole body and TA muscle weights were measured. *n* ≥ 3 mice of each genotype were examined. Mean ± s.d. values are shown in the dot-bar plot, and significance was determined by two-tailed student's t-test. ns: not significant.

(C) The TA myofiber size appeared normal in Ctrl and mutants with indicated genotypes. Cross sections of TA muscles were stained with anti-Laminin and DAPI. *n* ≥ 3 mice of each genotype were examined with similar results. Scale bar: 100 μm.

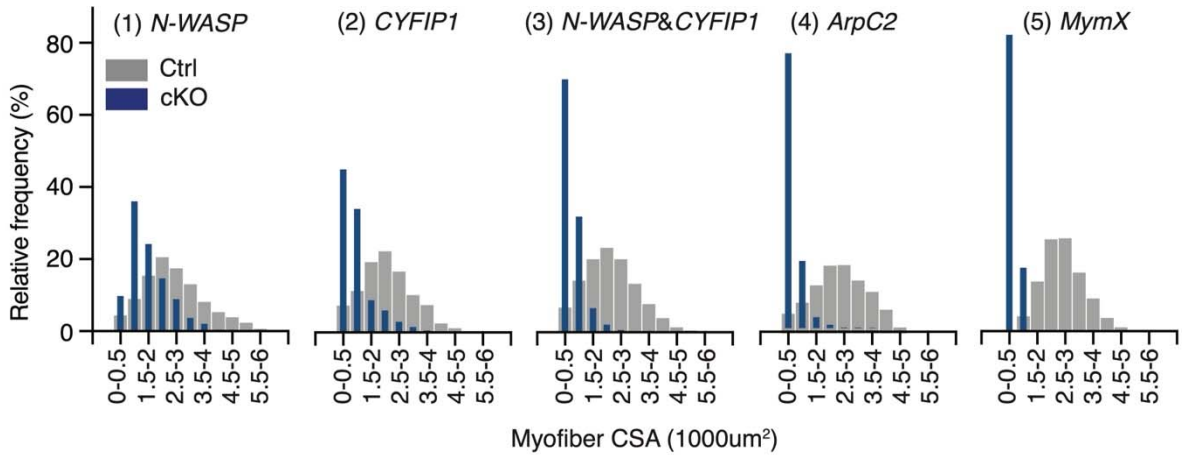

Supplementary Figure 2. Frequency distribution of myofiber CSA of TA muscles in the control and mutant mice at dpi 14. *n* = 3 mice of each genotype were examined and >500 ghost fibers in each mouse were examined.

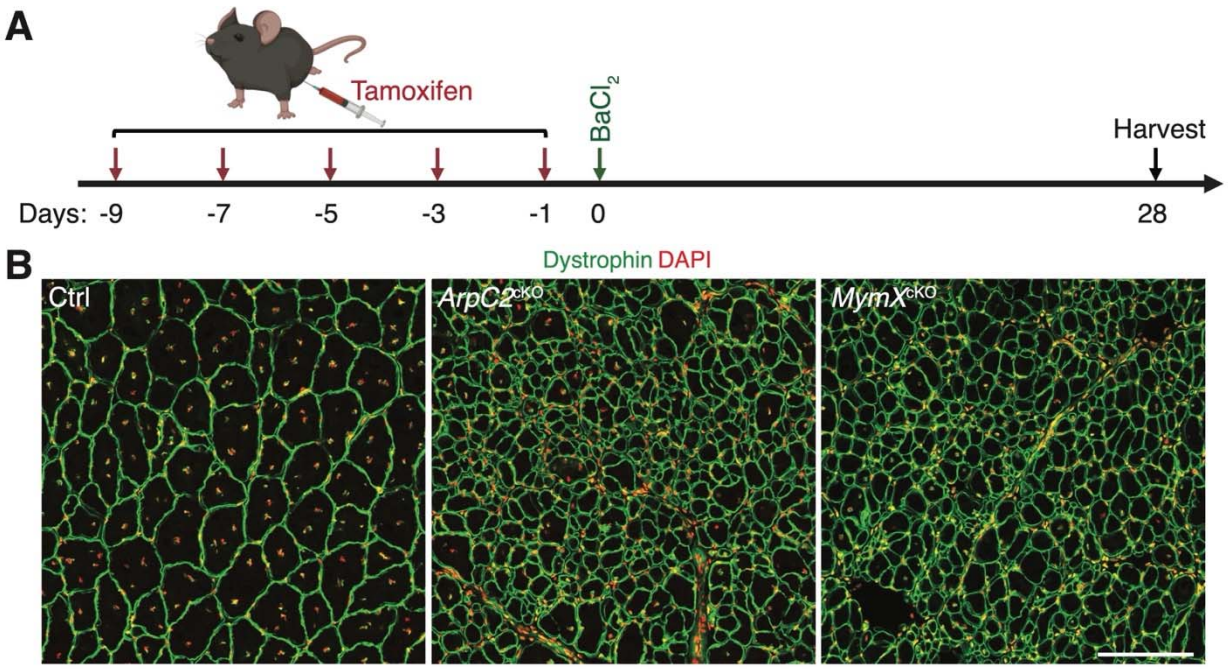

Supplementary Figure 3. Impaired muscle regeneration in *ArpC2*^{cKO} and *MymX*^{cKO} mice persists to dpi 28.

(A) Schematic diagram of tamoxifen and $BaCl_2$ treatment and subsequent CSA analysis at dpi 28.

(B) Dystrophin and DAPI staining in TA muscle cross sections at dpi 28 in the control and mutant mice. Note that the myofiber CSA is severely reduced in *ArpC2*^{cKO} and *MymX*^{cKO} mice compared to the control. Scale bar: 100 μm.

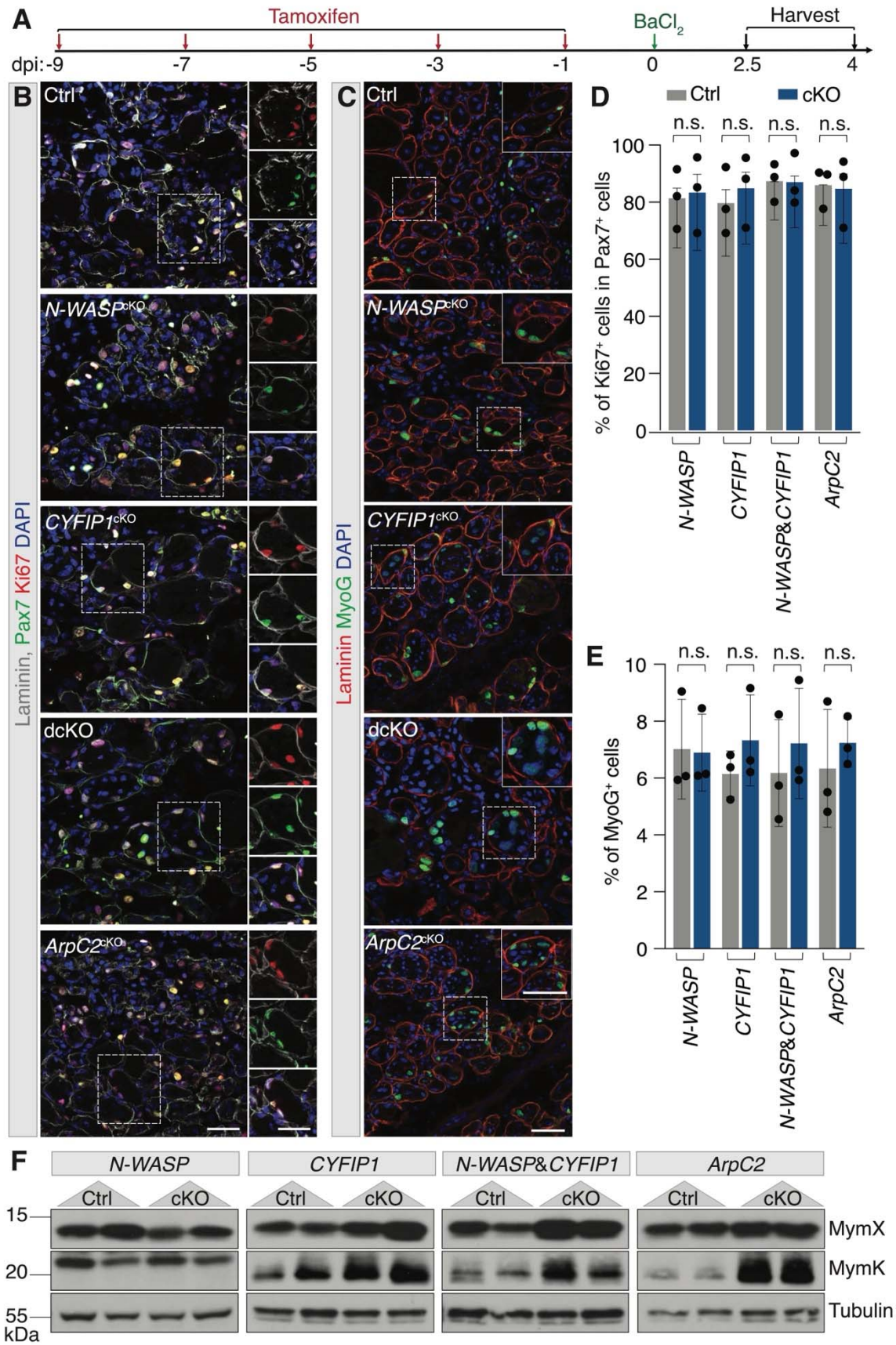

Supplementary Figure 4. Branched actin polymerization is not required for SC proliferation, differentiation, or fusogenic protein expression

(A) Schematic diagram of tamoxifen and $BaCl_2$ treatment and subsequent cell proliferation and differentiation analyses at dpi 2.5 and 4, respectively.

(B) Immunostaining with anti-Laminin, anti-Pax7 and anti-Ki67 of cross sections of TA muscles from control and mutant mice at dpi 2.5. The boxed the areas are shown at the bottom. Scale bar: 30 μm.

(C) Immunostaining with anti-Laminin and anti-MyoG of cross sections of TA muscles from control and mutant mice at dpi 4. The boxed areas are shown at the top right corner. Scale bar: 30 μm.

(D) Quantification of the percentage of proliferating SCs (% of $Ki67^+$ cells in the $Pax7^+$ cells) in TA muscles from control and mutant mice of the indicated genotypes.

(E) Quantification of the percentage of $MyoG^+$ nuclei in the total cells in TA muscles from control and mutant mice of the indicated genotypes.

(F) Western blot analysis for MymK and MymX in TA muscles from control and mutant mice of the indicated genotypes at dpi 4. Two samples of each control and mutant genotype were loaded.

For (**C**) and (**E**), *n* = 3 mice of each genotype were examined. Cells in 12 40x microscopic fields of each mouse were examined. Mean ± s.d. values are shown in the bar graph, and significance was determined by two-tailed student's t-test. ns: not significant.

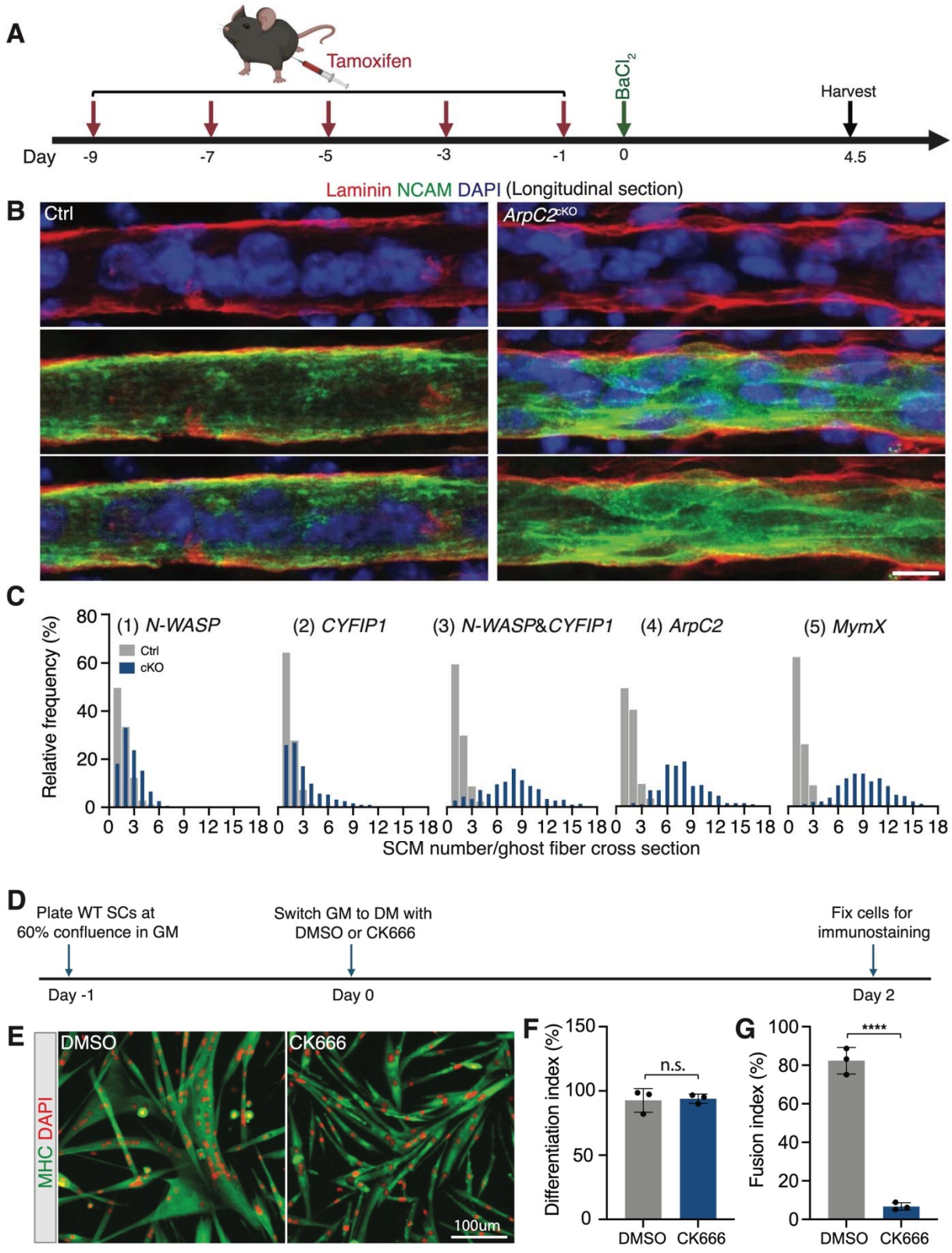

Supplementary Figure 5. Branched actin polymerization is required for SCM fusion

(A) Schematic diagram of tamoxifen and $BaCl_2$ treatment and subsequent SCM fusion analyses at dpi 4.5.

(B) Immunostaining with anti-Laminin and anti-NCAM of longitudinal sections of TA muscles from control and *ArpC2*^{cKO} mice. Scale bar: 10 μm.

(C) Frequency distribution of SCM number per ghost fiber from TA muscles of the indicated mutant mice and their littermate control. *n* = 3 mice of each genotype were analyzed and >500 ghost fibers in each mouse were examined.

(D) Schematic diagram of pharmacological inhibition of the Arp2/3 complex in wild-type SCs during differentiation. The wild-type SCs were plated at 60% confluence in GM, and switched to DM after a day. The cells were then incubated in DM supplemented with DMSO as a control (0.1%) or the Arp2/3 complex inhibitor CK666 (100 μM) for 48 hours, followed by anti-MHC and DAPI staining.

(E) MHC and DAPI staining of the cells described in (D). Note the robust fusion of control SCMs vs. the severe fusion defects in SCMs treated with CK666. Scale bar: 100 μm.

(F and **G)** Quantification of the differentiation and fusion indexes of the cells shown in (**D**). *n* = 3 independent experiments were performed.

For (**F**) and (**G**), Mean ± s.d. values are shown in the dot-bar graphs, and significance was determined by two-tailed student's t-test. ****: $p < 0.0001$; n.s: not significant.

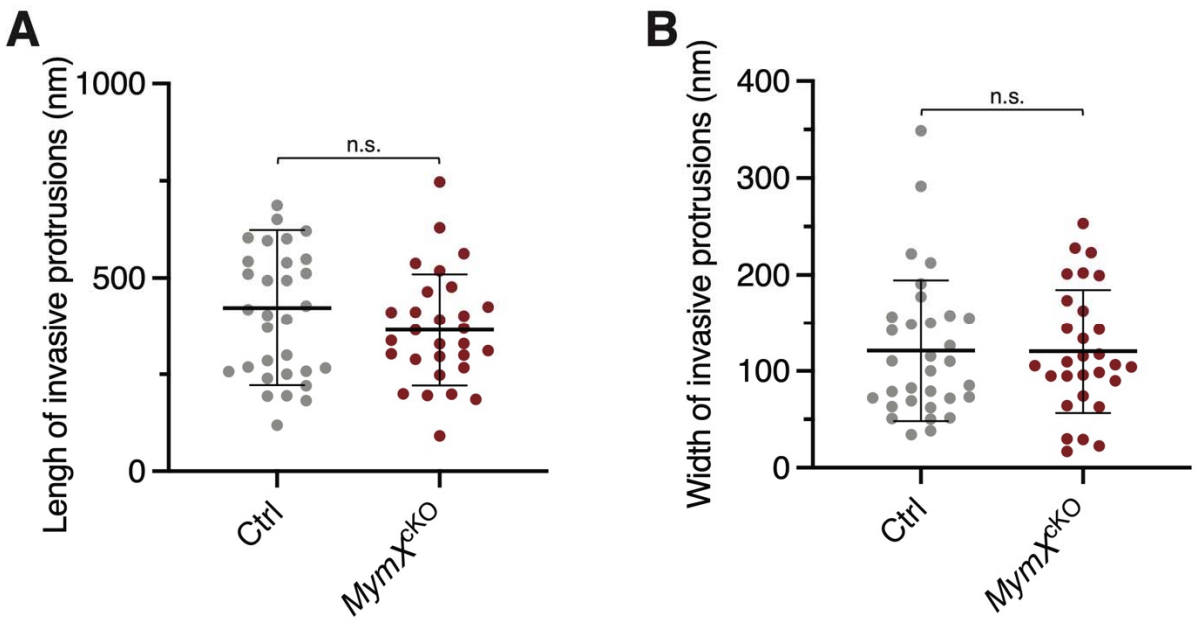

Supplementary Figure 6. Fusogenic protein MymX is not required for invasive protrusion formation

Quantification of the length (**A**) and width (**B**) of the invasive protrusions in control and *MymX*^{cKO} mice at dpi 3.5 imaged by TEM. The width was measured at the midpoints of the invasive protrusions. Mean ± s.d. values are shown in dot plots, and statistical analysis was performed for each parameter in $n \geq 29$ invasive protrusions in each genotype. n.s.: not significant.

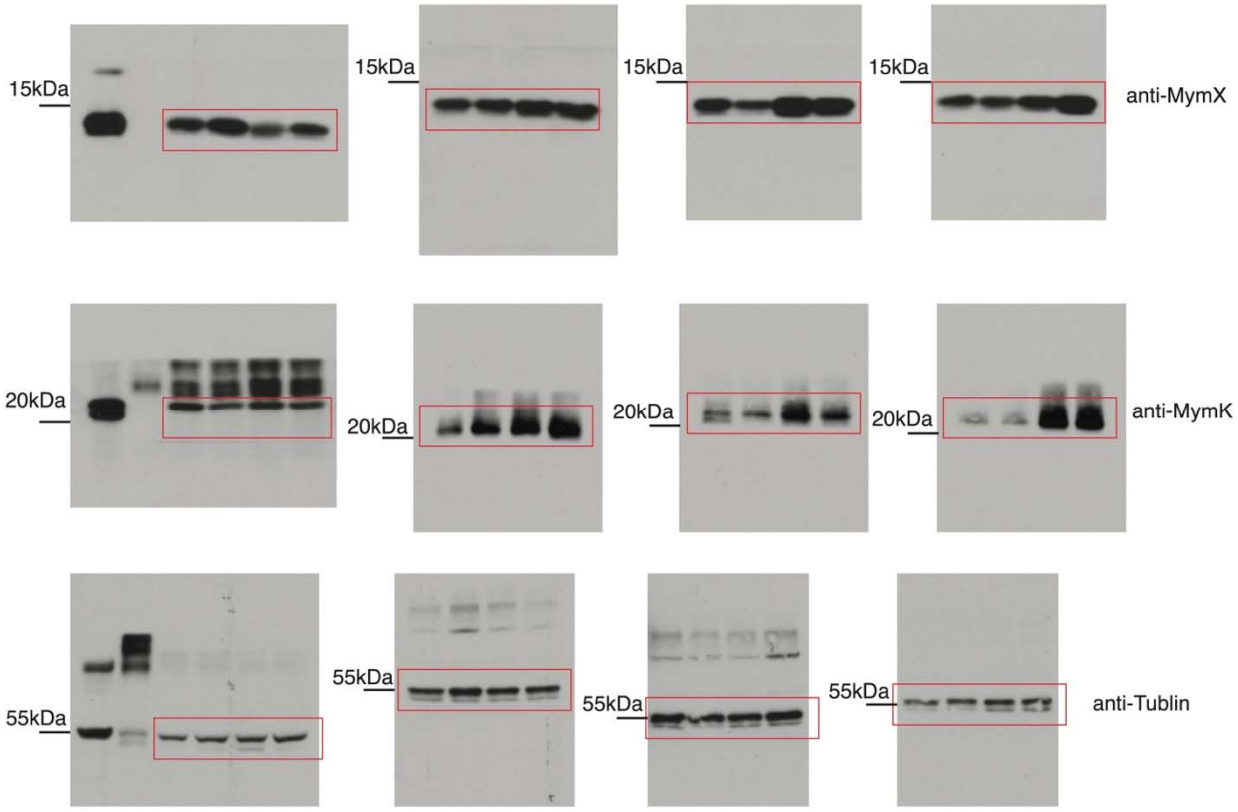

Supplementary Figure 7. Unprocessed western blot films

The unprocessed western blot films used to generate the Fig. S4F. The bands shown in Fig. S4F are highlighted by red boxes.

Supplemental Video 1 and 2. Macrophages extravasate the ghost fibers by traversing the BM

Representative 3D reconstruction of confocal z-stacks of TA muscle at dpi 3.5. Two examples are shown. The small opening on the BM is indicated by yellow arrowheads, and the transversing macrophage is indicated by magenta arrows.

Supplemental Video 3. Branched actin polymerization is not required for SCM migration during differentiation.

Time-lapse imaging of control and *ArpC2* KO SCs at 24 hours in DM. The SCs isolated from *ArpC2*^{cKO} mice were maintained in GM without or with 2 μM 4OH-tamoxifen (4OHT) for 10 days. Subsequently, the cells were plated in 70% confluence in GM. After 24 hours, the cells were cultured in DM for 12 hours, followed by live cell imaging. Note that the *ArpC2* KO SCMs were able to migrate normally, although their fusion was significantly impaired. The time interval is five minutes.

Supplemental Video 4. F-actin and the Arp2/3 complex are enriched in the invasive protrusions at the fusogenic synapse of SCMs

Time-lapse imaging of a fusion event between two mouse SCMs co-expressing LifeAct-mScar and Arp2-mNG at 24 hours in DM. Note that F-actin and Arp2 were enriched in the finger-like invasive protrusions at the fusogenic synapse (arrows) and dissolved immediately after cell membrane fusion. The time interval is two minutes. Single focal plane is shown.

Acknowledgements

We thank Dr. Eric Olson for generously providing the *MymX*$^{fl/fl}$ mice, UT Southwestern Animal Resource Center for assistance with mouse colony maintenance, and UT Southwestern Quantitative Light Microscopy Core Facility for assistance with 3D reconstruction of confocal images. This work was supported by an NIH grant (R35GM136316) to E.H.C.

Author contributions

Y.L. and E.H.C. designed the project. Y.L., T.W., P.P., and C.Z. performed experiments. Y.L., and E.H.C. analyzed the data, made the figures, and wrote the manuscript. All authors commented on the manuscript.

Data availability

The data supporting the findings of this study are available within the article and its supplementary files.

Declaration of interests

The authors declare no competing financial interests. Correspondence and requests for materials should be addressed to E.H.C. (Elizabeth.Chen@UTSouthwestern.edu) and Y.L. (Yue.Lu@UTSouthwestern.edu).

References

Bi P, McAnally JR, Shelton JM, Sanchez-Ortiz E, Bassel-Duby R, Olson EN. 2018. Fusogenic micropeptide Myomixer is essential for satellite cell fusion and muscle regeneration. *Proc Natl Acad Sci U S A* **115**: 3864-3869.

Capkovic KL, Stevenson S, Johnson MC, Thelen JJ, Cornelison DD. 2008. Neural cell adhesion molecule (NCAM) marks adult myogenic cells committed to differentiation. *Exp Cell Res* **314**: 1553-1565.

Carman CV, Sage PT, Sciuto TE, de la Fuente MA, Geha RS, Ochs HD, Dvorak HF, Dvorak AM, Springer TA. 2007. Transcellular diapedesis is initiated by invasive podosomes. *Immunity* **26**: 784-797.

Chen B, Brinkmann K, Chen Z, Pak CW, Liao Y, Shi S, Henry L, Grishin NV, Bogdan S, Rosen MK. 2014. The WAVE regulatory complex links diverse receptors to the actin cytoskeleton. *Cell* **156**: 195-207.

Chen B, Shan T. 2019. The role of satellite and other functional cell types in muscle repair and regeneration. *J Muscle Res Cell Motil* **40**: 1-8.

Chen EH. 2011. Invasive podosomes and myoblast fusion. *Curr Top Membr* **68**: 235-258.

Cheung TH, Rando TA. 2013. Molecular regulation of stem cell quiescence. *Nat Rev Mol Cell Biol* **14**: 329-340.

Collins BC, Shapiro JB, Scheib MM, Musci RV, Verma M, Kardon G. 2024. Three-dimensional imaging studies in mice identify cellular dynamics of skeletal muscle regeneration. *Dev Cell*.

Cotta-de-Almeida V, Westerberg L, Maillard MH, Onaldi D, Wachtel H, Meelu P, Chung UI, Xavier R, Alt FW, Snapper SB. 2007. Wiskott Aldrich syndrome protein (WASP) and N-WASP are critical for T cell development. *Proc Natl Acad Sci U S A* **104**: 15424-15429.

Faust JJ, Balabiyev A, Heddleston JM, Podolnikova NP, Baluch DP, Chew TL, Ugarova TP. 2019. An actin-based protrusion originating from a podosome-enriched region initiates macrophage fusion. *Mol Biol Cell* **30**: 2254-2267.

Goley ED, Welch MD. 2006. The ARP2/3 complex: an actin nucleator comes of age. *Nat Rev Mol Cell Biol* **7**: 713-726.

Grefte S, Kuijpers-Jagtman AM, Torensma R, Von den Hoff JW. 2007. Skeletal muscle development and regeneration. *Stem Cells Dev* **16**: 857-868.

Gruenbaum-Cohen Y, Harel I, Umansky KB, Tzahor E, Snapper SB, Shilo BZ, Schejter ED. 2012. The actin regulator N-WASp is required for muscle-cell fusion in mice. *Proc Natl Acad Sci U S A* **109**: 11211-11216.

Habela CW, Yoon KJ, Kim NS, Taga A, Bell K, Bergles DE, Maragakis NJ, Ming GL, Song H. 2020. Persistent Cyfip1 Expression Is Required to Maintain the Adult Subventricular Zone Neurogenic Niche. *J Neurosci* **40**: 2015-2024.

Hohsfield LA, Tsourmas KI, Ghorbanian Y, Syage AR, Jin Kim S, Cheng Y, Furman S, Inlay MA, Lane TE, Green KN. 2022. MAC2 is a long-lasting marker of peripheral cell infiltrates into the mouse CNS after bone marrow transplantation and coronavirus infection. *Glia* **70**: 875-891.

Kim JH, Chen EH. 2019. The fusogenic synapse at a glance. *J Cell Sci* **132**.

Kim JH, Jin P, Duan R, Chen EH. 2015a. Mechanisms of myoblast fusion during muscle development. *Curr Opin Genet Dev* **32**: 162-170.

Kim JH, Ren Y, Ng WP, Li S, Son S, Kee YS, Zhang S, Zhang G, Fletcher DA, Robinson DN et al. 2015b. Mechanical tension drives cell membrane fusion. *Dev Cell* **32**: 561-573.

Le Grand F, Rudnicki MA. 2007. Skeletal muscle satellite cells and adult myogenesis. *Curr Opin Cell Biol* **19**: 628-633.

Lee DM, Chen EH. 2019. Drosophila Myoblast Fusion: Invasion and Resistance for the Ultimate Union. *Annu Rev Genet* **53**: 67-91.

Lepper C, Conway SJ, Fan CM. 2009. Adult satellite cells and embryonic muscle progenitors have distinct genetic requirements. *Nature* **460**: 627-631.

Lu Y, Walji T, Ravaux B, Pandey P, Li B, Lam KH, Zhang R, Goldhamer DJ, Li R, Schmidtke DW et al. 2023. Molecular Regulation of Invasive Protrusion Formation at the Mammalian Fusogenic Synapse. *bioRxiv*: 2023.2011.2027.568897.

Luo Z, Shi J, Pandey P, Ruan ZR, Sevdali M, Bu Y, Lu Y, Du S, Chen EH. 2022. The cellular architecture and molecular determinants of the zebrafish fusogenic synapse. *Dev Cell* **57**: 1582-1597 e1586.

Millay DP, Sutherland LB, Bassel-Duby R, Olson EN. 2014. Myomaker is essential for muscle regeneration. *Genes Dev* **28**: 1641-1646.

Relaix F, Zammit PS. 2012. Satellite cells are essential for skeletal muscle regeneration: the cell on the edge returns centre stage. *Development* **139**: 2845-2856.

Richardson BE, Beckett K, Nowak SJ, Baylies MK. 2007. SCAR/WAVE and Arp2/3 are crucial for cytoskeletal remodeling at the site of myoblast fusion. *Development* **134**: 4357-4367.

Seale P, Sabourin LA, Girgis-Gabardo A, Mansouri A, Gruss P, Rudnicki MA. 2000. Pax7 is required for the specification of myogenic satellite cells. *Cell* **102**: 777-786.

Sens KL, Zhang S, Jin P, Duan R, Zhang G, Luo F, Parachini L, Chen EH. 2010. An invasive podosome-like structure promotes fusion pore formation during myoblast fusion. *J Cell Biol* **191**: 1013-1027.

Shilagardi K, Li S, Luo F, Marikar F, Duan R, Jin P, Kim JH, Murnen K, Chen EH. 2013. Actin-propelled invasive membrane protrusions promote fusogenic protein engagement during cell-cell fusion. *Science* **340**: 359-363.

Wang PS, Chou FS, Ramachandran S, Xia S, Chen HY, Guo F, Suraneni P, Maher BJ, Li R. 2016. Crucial roles of the Arp2/3 complex during mammalian corticogenesis. *Development* **143**: 2741-2752.

Webster MT, Manor U, Lippincott-Schwartz J, Fan CM. 2016. Intravital Imaging Reveals Ghost Fibers as Architectural Units Guiding Myogenic Progenitors during Regeneration. *Cell Stem Cell* **18**: 243-252.

Yin H, Price F, Rudnicki MA. 2013. Satellite cells and the muscle stem cell niche. *Physiol Rev* **93**: 23-67.

Zhang H, Wen J, Bigot A, Chen J, Shang R, Mouly V, Bi P. 2020. Human myotube formation is determined by MyoD-Myomixer/Myomaker axis. *Sci Adv* **6**.

Zhang S, Chen EH. 2008. Ultrastructural analysis of myoblast fusion in Drosophila. *Methods Mol Biol* **475**: 275-297.